

LoRAP: Low-Rank Aggregation Prompting for Quantized Graph Neural Networks Training

Chenyu Liu¹, Haige Li¹, Luca Rossi¹

¹The Hong Kong Polytechnic University

chen-yu.liu@connect.polyu.hk, luca.rossi@polyu.edu.hk

Abstract

Graph Neural Networks (GNNs) are neural networks that aim to process graph data, capturing the relationships and interactions between nodes using the message-passing mechanism. GNN quantization has emerged as a promising approach for reducing model size and accelerating inference in resource-constrained environments. Compared to quantization in LLMs, quantizing graph features is more emphasized in GNNs. Inspired by the above, we propose to leverage prompt learning, which manipulates the input data, to improve the performance of quantization-aware training (QAT) for GNNs. To mitigate the issue that prompting the node features alone can only make part of the quantized aggregation result optimal, we introduce Low-Rank Aggregation Prompting (LoRAP), which injects lightweight, input-dependent prompts into each aggregated feature to optimize the results of quantized aggregations. Extensive evaluations on 4 leading QAT frameworks over 9 graph datasets demonstrate that LoRAP consistently enhances the performance of low-bit quantized GNNs while introducing a minimal computational overhead.¹

1 Introduction

Graph Neural Networks (GNNs) are models able to process graph data, effectively capturing the node relationships using the message-passing mechanism. This ability allows GNNs to model complex dependencies and interactions present in graphs and enabled their application in several domains, such as biology [Hetzell *et al.*, 2021], chemistry [Reiser *et al.*, 2022; Minello *et al.*, 2025], recommender systems [Wu *et al.*, 2022], and network analysis [Tang and Liu, 2010; Rahmani *et al.*, 2023]. Despite their wide use, the adoption of GNNs in resource-constrained environments, such as mobile phones, autonomous vehicles, and edge devices, is still challenging [Wu *et al.*, 2022]. Even though they have fewer parameters than standard deep learning models, GNNs typically involve more computations, often exceeding the computational cost of standard models [Tailor, 2020]. This, in turn, is largely driven by the size of the underlying graph.

When dealing with large neural networks, particularly large language models (LLMs), model quantization has emerged as a promising approach to handle their deployment in resource-constrained environments [Dettmers *et al.*, 2022]. This in turn involves representing weights and activations with lower precision, reducing the model size and accelerating inference. While traditional quantization techniques focus primarily on the weights of the model, in the case of GNNs the quantization of node features and graph structure becomes significantly more important. As the graph scale increases, the necessary storage size escalates dramatically, severely impacting the limited memory budget of resource-constrained devices. In contrast, memory consumption in LLMs is overwhelmingly dominated by parameter weights. Feature representations can comprise up to 98.44% of the total memory footprint of a GNN [Feng *et al.*, 2020], whereas in LLaMA-2-7B roughly 87% of the overall memory usage is attributable to model weights [Li *et al.*, 2023]. Note also that GNN inference involves repeated message passing over node embeddings, thus any reduction in the bit-width of node data directly shrinks memory transfers and arithmetic operations on each edge, yielding substantial speedups and bandwidth savings in real-world deployments. The reduced memory footprint and runtime, however, usually result in decreased performance on downstream tasks. This drop is particularly pronounced when quantization is applied to GNNs, where the relationships between nodes and their neighbors are crucial for effective learning. For this reason, several approaches have been introduced to incorporate quantization-aware training (QAT) for GNNs. These methods try to mitigate quantization errors by leveraging node degree information [Tailor, 2020] or using mixed-precision strategies [Zhu *et al.*, 2023]. Despite this, quantizing GNNs to low-bit representations still incurs a large accuracy drop. Since quantization errors in GNNs primarily arise from feature quantization and accumulate in deeper layers, in this paper we propose to use prompt learning, a technique where additional learnable parameters are injected into data features, to mitigate the performance degradation of quantized GNNs. Prompt tuning was introduced as a technique to recover the performance of compressed LLMs [Xu *et al.*, 2024], with most methods in this context being adapter-based [Dettmers *et al.*, 2024],

¹Code available at anonymous.4open.science/r/LoRAP-16F3/

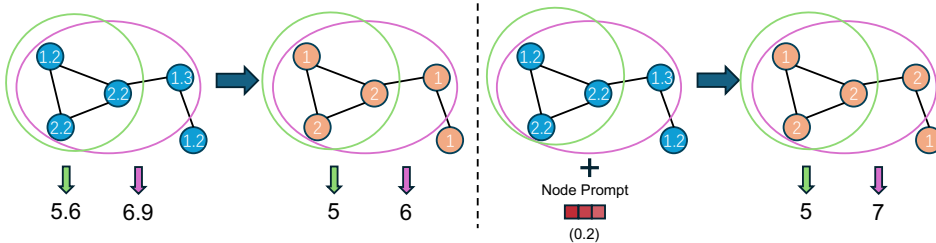


Figure 1: (Left) The aggregation phase in a full-precision GNN and its quantized version. (Right) The aggregation phase in a full-precision prompt-tuned GNN (where a node prompt with a value of 0.2 is added) and its quantized version. The neighbourhoods where the aggregations take place are denoted by green & magenta circles, respectively, with the aggregated values indicated by green & magenta arrows, respectively.

since quantization in LLMs emphasizes weights. However, extending this approach to GNN models is not straightforward and incurs considerable challenges [Fang *et al.*, 2024]. To this end, in this paper we first propose to recover the performance of quantized GNNs by incorporating prompts in the node features space. We implement GPF-plus [Fang *et al.*, 2024] for QAT, which integrates different prompted features for each node in the graph. However, adding node prompts can only make part of the quantized aggregation result optimal, as shown in Fig. 1 (Right). To alleviate this issue while keeping our approach as simple as possible, we propose to insert prompts over node aggregations, thereby reducing the quantization error incurred by low-precision node representations. Our prompts are also designed to be input-dependent and computationally efficient, making use of low-rank basis matrices. Our contributions can be summarized as follows:

- We are the first to leverage prompt learning to improve the performance of quantized GNN models. Specifically, we manipulate the node features, the major source of reduced performance in quantized GNNs.
- We propose LoRAP, a **Low-Rank Aggregation Prompting** strategy where we insert input-dependent computationally efficient prompts over node feature aggregations, improving the quantized aggregation results; Moreover, to reduce the latency, we propose to fuse the GPU operations in LoRAP, resulting in the fused LoRAP kernel.
- Experiments on 4 QAT frameworks for GNNs over a wide variety of datasets demonstrate that combining GPF-plus and LoRAP consistently increases the model performance.

2 Fundamentals of Graph Neural Networks

Unlike traditional convolutional neural networks that operate on grid-like data, GNNs leverage the graph topology to propagate information across nodes, enabling the model to learn representations that capture the relational inductive biases inherent in graphs. Consider a graph $\mathcal{G} = (\mathcal{V}, \mathcal{E})$ consisting of a set of nodes $\mathcal{V} = \{v_1, v_2, \dots, v_N\}$ and edges \mathcal{E} , where each node v_i is associated with a feature vector $\mathbf{x}_i \in \mathbb{R}^d$. Let $\mathbf{X} = [\mathbf{x}_1; \mathbf{x}_2; \dots; \mathbf{x}_N] \in \mathbb{R}^{N \times d}$ be the matrix of these features and $\mathbf{A} \in \mathbb{R}^{N \times N}$ be the adjacency matrix encoding the connectivity between nodes, where \mathbf{A}_{ij} denotes the presence (and possibly the weight) of an edge between nodes v_i and v_j . The message passing mechanism at the core of GNNs

consists of three key phases: message passing, aggregation, and node update. In the message passing phase, each node v_i sends a message to its neighbors based on its current state and edge information. The message from node v_i to its neighbor v_j is computed as a function ϕ that depends on the node features and the edge features, *i.e.*,

$$\mathbf{m}_{ij} = \phi \left(\mathbf{h}_i^{(l)}, \mathbf{h}_j^{(l)}, \mathbf{e}_{ij} \right),$$

where $\mathbf{h}_i^{(l)}$ and $\mathbf{h}_j^{(l)}$ are the features of v_i and v_j at layer l and \mathbf{e}_{ij} represents the edge feature between v_i and v_j . In the aggregation phase, the messages received from neighbors are combined into a single message for each node. The aggregation function \wedge is typically permutation-invariant, ensuring that the order of neighbors does not affect the result. The aggregated message for node v_i can be expressed as

$$\mathbf{s}_i = \bigwedge_{j \in \mathcal{N}(i)} \mathbf{m}_{ij} = \bigwedge_{j \in \mathcal{N}(i)} \phi \left(\mathbf{h}_i^{(l)}, \mathbf{h}_j^{(l)}, \mathbf{e}_{ij} \right),$$

where $\mathcal{N}(i)$ is the set of neighbors of node v_i , and \bigwedge can be a sum, mean, or max function, depending on the architecture. Each node finally updates its representation based on its current features and the aggregated messages, typically using a learnable function γ , such as a multi-layer perceptron. The update rule for node v_i at layer $l + 1$ is

$$\mathbf{h}_i^{(l+1)} = \gamma \left(\mathbf{h}_i^{(l)}, \mathbf{s}_i \right).$$

3 Prompt Tuning For Quantized GNNs

3.1 Node feature compression

Given an unweighted graph \mathcal{G} , the quantization process is typically formulated as an optimization problem where one aims to minimize the reconstruction error between the original node-feature matrix $\mathbf{X} \in \mathbb{R}^{N \times d}$ and its quantized counterpart $Q(\mathbf{X}) \in \mathbb{R}^{N \times d}$ [Zhu *et al.*, 2023]. Accordingly, the feature-quantization loss is defined as

$$\arg \min_Q \|\mathbf{X} - Q(\mathbf{X})\|_F, \quad (1)$$

which directly measures the Frobenius-norm difference under a fixed-bit budget. The goal is to optimize the parameters of the quantizer $Q(\cdot)$ in order to minimize this loss. However, directly minimizing the feature-quantization loss disregards the graph propagation dynamics. As shown in Fig. 1

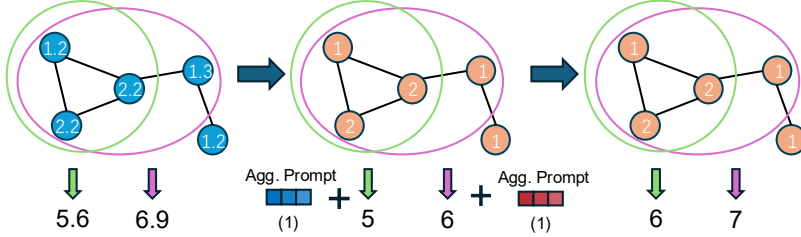


Figure 2: The aggregation prompting strategy. After quantizing the full-precision GNN model, we add input-dependent prompts to each aggregation, thus minimizing the aggregation-quantization loss.

(Left), consider the case where we quantize node features using a round-to-nearest (RTN) approach. Although the feature-quantization loss is minimized, the resulting quantized aggregated features still fail to closely approximate those obtained under full-precision quantization. To remedy this issue, here we propose to introduce an aggregation-quantization loss that measures the discrepancy between the aggregated feature matrix of the full-precision and quantized GNNs,

$$\arg \min_Q \|f(\mathbf{X}, \mathbf{A}) - f(Q(\mathbf{X}), \mathbf{A})\|_F, \quad (2)$$

where $f(\mathbf{X}, \mathbf{A})_i$ denotes the aggregation result produced by the GNN with input features \mathbf{X} and adjacency matrix \mathbf{A} .

3.2 Prompt tuning minimizes quantization loss

Different from prompt tuning in NLP, where learnable tokens are appended to the input sequence, applying prompt tuning in GNNs is more complex due to the non-trivial structure of graphs [Liu and Rossi, 2025]. In this work, we claim that soft prompts can minimize the quantized approximation error in (see Appendix A.2, Theorem 3). Inspired by the success of pixel-level visual prompt techniques in computer vision [Bahng *et al.*, 2022], a natural extension of this approach in graph-based models is GPF, which integrates learnable prompts directly into the node features [Fang *et al.*, 2023]. This can be achieved by adding trainable components to the graph node feature space, allowing the model to adaptively modify the feature representations during the learning process. We denote this approach as **node prompting**.

Given a graph \mathcal{G} , node prompting uses GPF to add a shared learnable prompt vector $\mathbf{p} \in \mathbb{R}^d$ to each node feature vector,

$$\tilde{\mathbf{x}}_i = \mathbf{x}_i + \mathbf{p}, \quad \forall i \in \mathcal{V},$$

where $\tilde{\mathbf{x}}_i$ denotes the prompted feature vector for node i , and \mathbf{x}_i is the original feature vector. This addition modifies the input features without altering the model parameters. In real-world quantization, we do not rely on simple RTN quantization. Instead, more sophisticated strategies are employed, which incorporate learnable quantization parameters such as scale (S) and zero-point (Z) [Esser *et al.*, 2020]. By learning the scale and zero-point parameters, these strategies can reduce quantization loss and better preserve the precision of the model representation. Incorporating prompt vectors into this process further enhances the ability to minimize the reconstruction loss, ensuring that the quantized features align more closely with the full-precision values. For instance,

when quantizing features into low bits, it is possible to observe $\|\mathbf{X} - Q(\mathbf{X})\|_F \gg 0$. However, by incorporating high-precision node prompts \mathbf{P} , we can jointly optimize the quantization function and learnable prompts, thereby reducing the feature quantization loss to a level near zero, *i.e.*,

$$\arg \min_{Q, \mathbf{P}} \| \mathbf{X} - (Q(\mathbf{X}) + \mathbf{P}) \|_F \approx 0 \quad (3)$$

While GPF minimizes the feature-quantization loss (Eq. 1), this does not hold true for the aggregation-quantization loss (Eq. 2). In Fig. 1 (Left), we show two examples of aggregations (in sum) denoted by a green circle and a magenta circle, respectively. The result of the full-precision aggregation is 6.9 and 5.6 for the magenta and green circles, respectively. If we consider instead the case where the node features are quantized using RTN, the aggregation result is 6 and 5, respectively. Note however that these quantized aggregations are far from the optimal ones (7 and 6). Fig. 1 (Right) illustrates what happens if we try to alleviate this issue using the node prompting strategy. By adding a prompt \mathbf{p} with value 0.2 to each node during the tuning phase we can make the aggregation result for the magenta circle optimal, however the same cannot be achieved for the green circle. In other words, GPF is only able to minimize the aggregation-loss to a limited extent. [Zhu *et al.*, 2023] identifies the aggregation phase as a significant source of numerical error. We propose to mitigate this issue by introducing a new strategy named **aggregation prompting** where we add prompts over the aggregated features, *e.g.*, we can add a prompt \mathbf{p} with value 1 to each quantized aggregation to bring them closer to their optimal quantized values (see Fig. 2). The advantage of aggregation prompting over traditional node-level prompts lies in its ability to directly influence the aggregation process, ensuring that the final feature representations better align with the optimal values. We therefore state the following theorem by defining our aggregation prompting as **post-aggregation prompting**, and previous prompting methods like GPF as **pre-aggregation prompting** (proof in the Appendix A.2, Theorem 1).

Theorem 1 (Optimization Decoupling) *In post-aggregation prompting ($AX_q + P$), the optimal prompt P_{post}^* directly compensates for the propagated quantization error $A\epsilon_X$ and its learning objective is decoupled from the graph aggregation operator A . In contrast, in pre-aggregation prompting ($A(X_q + P)$), the learning objective for the optimal prompt P_{pre}^* is deeply coupled with A , requiring the model to learn a complex, topology-dependent “pre-inverse” transformation.*

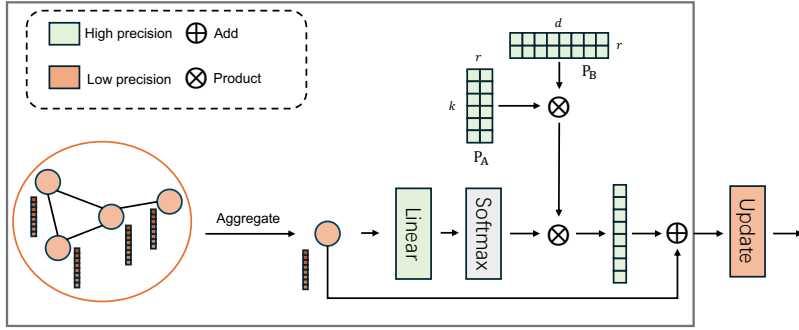


Figure 3: To insert low-rank prompts in an aggregation, we first get the aggregated feature for a set of quantized nodes. Then the aggregated feature is used to perform a weighted sum of the basis vectors (composed of low-rank matrices) to produce the prompt. The prompt is then added to the aggregated feature. The prompt generation procedure is in high-precision, other GNN operations are in low-precision.

Moreover, by applying prompts to the aggregated features, our method allows the model to focus on adjusting the combined information from neighboring nodes, leading to a more accurate and refined output after quantization. This targeted adjustment helps mitigate the loss of precision that typically occurs when quantizing individual node features, resulting in better performance (proof in the Appendix A.2, Theorem 2).

Theorem 2 (Targeted Correction Capability) *In GNN quantization, systematic bias caused by high-in-degree nodes is a primary source of error. Post-aggregation prompting ($AX_q + P$) can directly and specifically correct the systematic bias in the aggregated message of node i by learning a node-specific row vector P_i . In contrast, pre-aggregation prompting ($A(X_q + P)$) cannot achieve such targeted correction because the prompt vector P_i for node i primarily affects the aggregated messages of its neighbors, not its own.*

4 Low-Rank Aggregation Prompt Tuning

Fig. 3 illustrates the proposed method, whose components are discussed in the following subsections.

4.1 Aggregation prompt insertion

Instead of introducing additional learnable parameters into the feature space of the input graph as in [Fang *et al.*, 2023], our approach is to insert prompts into the aggregated features. Specifically, during the aggregation phase of a GNN layer, we add a learnable prompt vector $\mathbf{p} \in \mathbb{R}^d$ to the set of aggregated features $\mathbf{S} = \{\mathbf{s}_1, \mathbf{s}_2, \dots, \mathbf{s}_N\}$ of the nodes, *i.e.*,

$$\mathbf{S}^* = \{\mathbf{s}_1 + \mathbf{p}, \mathbf{s}_2 + \mathbf{p}, \dots, \mathbf{s}_N + \mathbf{p}\}, \quad (4)$$

where \mathbf{S}^* is the set of manipulated aggregated features that aims to reduce the aggregation-quantization loss, *i.e.*,

$$\arg \min_{Q, \mathbf{P}} \|f(\mathbf{X}, \mathbf{A}) - (f(Q(\mathbf{X}), \mathbf{A}) + \mathbf{P})\|_F \approx 0. \quad (5)$$

By jointly optimizing the prompts \mathbf{P} and quantization function Q , the aggregation-quantization error can be reduced to close to zero. Mathematically, The message passing paradigm can be reformulated as

$$\mathbf{h}_i^{(l+1)} = \gamma \left(\mathbf{h}_i^{(l)}, \bigwedge_{j \in \mathcal{N}(i)} \phi \left(\mathbf{h}_i^{(l)}, \mathbf{h}_j^{(l)}, \mathbf{e}_{ij} \right) + \mathbf{p} \right). \quad (6)$$

4.2 Input-dependent low-rank aggregation prompt

While aggregation prompting introduces a simple approach to embedding prompts, relying on a single shared prompt vector for all aggregations fails to account for the inherent diversity of aggregations taking place over different neighborhoods. To address this issue, we propose an extension where distinct, learnable prompt vectors are assigned to each aggregation, instead of using one uniform prompt vector \mathbf{p} . This allows the model to more precisely adjust to the unique characteristics of each aggregation operation. However, training a separate prompt vector for every aggregation is practically unfeasible, since there will be N aggregations in an aggregation phase. Specifically, for each layer l in a GNN with L layers, we learn a set of k prompt bases $\mathcal{P}^{(l)} = \{\mathbf{b}_1^{(l)}, \mathbf{b}_2^{(l)}, \dots, \mathbf{b}_k^{(l)}\}$, where each $\mathbf{b}_m^{(l)} \in \mathbb{R}^d$ and k is a hyperparameter. Note that $k \ll N$ in order to improve the parameter efficiency. We then propose to use a high-precision input-dependent linear function ϕ followed by a softmax to map the aggregated feature $\mathbf{s}_i^{(l)}$ to a probability distribution $\alpha_i^{(l)} \in \mathbb{R}^k$ where the element $\alpha_{im}^{(l)}$ represents the weight or importance of the corresponding basis prompt vector $\mathbf{b}_m^{(l)}$, *i.e.*,

$$\alpha_i^{(l)} = \text{Softmax}(\phi(\mathbf{s}_i^{(l)})). \quad (7)$$

The probabilities $\alpha_i^{(l)}$ are positive and ensure that the weights sum to 1, which means they can be interpreted as the relative importance of each basis vector in constructing the final output. In this paper, the linear layer ϕ is shared across all layers and we set different prompt sets $\mathbf{P}^{(l)}$ for every layer. Using these learned probabilities, the prompt $\mathbf{p}_i^{(l)} \in \mathbb{R}^d$ is defined as the convex combination of basis vectors

$$\mathbf{p}_i^{(l)} = \sum_{m=1}^k \alpha_{im}^{(l)} \mathbf{b}_m^{(l)}. \quad (8)$$

The generated prompt is input-dependent as it is dynamically formed by combining the learned basis vectors with weights that are produced based on the aggregation features.

In our implementation, the set of prompt bases is represented as a matrix $\mathbf{P}^{(l)} \in \mathbb{R}^{k \times d}$. As we have a matrix $\mathbf{P}^{(l)}$ for every layer, this introduces $L \times k \times d$ number of parameters. To improve the parameter efficiency, we decompose

Table 1: The results of 3 quantization frameworks with FP32 baselines at the top. We provide three quantization frameworks for INT4: standard QAT, Degree-Quant (DQ), and A^2Q . They are validated on 3 model architectures with 3 prompt strategies: (1) no prompts, (2) GPF-plus, and (3) GPF-LoRAP. We highlight in bold the improvement of GPF-LoRAP over non-prompting.

Quant. Frame.	Model Arch.	Prompt Method	Node Classification (Accuracy %)		Graph Classification (Accuracy %)		Graph Regression (Loss)
			Cora \uparrow	Citeseer \uparrow	MNIST \uparrow	CIFAR-10 \uparrow	ZINC \downarrow
FP32	GIN	None	77.6 \pm 1.1	66.1 \pm 0.9	96.4 \pm 0.4	53.3 \pm 3.7	0.414 \pm 0.009
	GCN	None	81.4 \pm 0.7	71.1 \pm 0.7	90.9 \pm 0.4	54.5 \pm 0.1	0.469 \pm 0.002
	GAT	None	83.1 \pm 0.4	72.5 \pm 0.7	95.8 \pm 0.4	65.4 \pm 0.4	0.463 \pm 0.002
QAT	GIN	None	44.2 \pm 1.5	18.7 \pm 3.7	91.0 \pm 0.5	48.7 \pm 1.7	0.555 \pm 0.024
	GIN	GPF-plus	45.6 \pm 3.0	21.6 \pm 2.9	91.3 \pm 0.3	55.3 \pm 0.9	0.569 \pm 0.020
	GIN	GPF-LoRAP	45.1 \pm 2.8 (+0.9)	22.8 \pm 4.8 (+4.1)	91.8 \pm 0.4 (+0.8)	55.8 \pm 0.5 (+7.1)	0.528 \pm 0.017 (+2.7)
DQ	GIN	None	61.0 \pm 6.9	58.4 \pm 2.1	92.4 \pm 0.4	50.7 \pm 1.6	0.540 \pm 0.019
	GIN	GPF-plus	64.3 \pm 5.0	63.1 \pm 3.5	91.9 \pm 0.3	51.3 \pm 1.2	0.555 \pm 0.018
	GIN	GPF-LoRAP	68.8 \pm 4.3 (+7.8)	64.6 \pm 2.3 (+6.2)	92.9 \pm 0.3 (+0.5)	53.0 \pm 0.9 (+2.3)	0.512 \pm 0.008 (+2.8)
A^2Q	GIN	None	77.4 \pm 0.9	66.6 \pm 0.1	95.7 \pm 0.2	54.9 \pm 0.9	0.400 \pm 0.016
	GIN	GPF-plus	72.7 \pm 0.8	59.5 \pm 6.6	95.9 \pm 0.4	56.8 \pm 1.4	0.399 \pm 0.009
	GIN	GPF-LoRAP	78.5 \pm 1.0 (+1.1)	70.7 \pm 0.6 (+4.1)	96.4 \pm 0.2 (+0.7)	57.4 \pm 1.4 (+2.5)	0.361 \pm 0.010 (+3.7)
QAT	GCN	None	66.4 \pm 7.0	63.4 \pm 2.2	70.6 \pm 2.4	38.5 \pm 1.3	0.707 \pm 0.056
	GCN	GPF-plus	69.8 \pm 6.5	61.6 \pm 3.1	71.5 \pm 1.3	41.0 \pm 1.2	0.733 \pm 0.018
	GCN	GPF-LoRAP	71.3 \pm 8.3 (+4.9)	63.9 \pm 2.2 (+0.5)	73.6 \pm 1.2 (+2.6)	43.6 \pm 1.3 (+5.1)	0.690 \pm 0.021 (+1.7)
DQ	GCN	None	72.5 \pm 3.7	68.6 \pm 3.3	87.0 \pm 1.2	49.5 \pm 0.8	0.657 \pm 0.032
	GCN	GPF-plus	72.3 \pm 2.8	71.4 \pm 3.1	90.9 \pm 0.7	51.1 \pm 0.5	0.534 \pm 0.017
	GCN	GPF-LoRAP	78.0 \pm 2.5 (+5.5)	71.0 \pm 2.9 (+2.4)	92.4 \pm 0.5 (+5.4)	53.4 \pm 0.5 (+3.9)	0.570 \pm 0.012 (+8.7)
A^2Q	GCN	None	76.1 \pm 0.3	69.7 \pm 1.6	90.5 \pm 0.5	52.4 \pm 0.8	0.504 \pm 0.009
	GCN	GPF-plus	78.0 \pm 0.1	70.0 \pm 2.3	91.0 \pm 0.5	53.2 \pm 1.0	0.506 \pm 0.008
	GCN	GPF-LoRAP	79.1 \pm 0.1 (+3.0)	71.8 \pm 0.7 (+2.1)	91.8 \pm 0.6 (+1.3)	53.5 \pm 1.2 (+1.1)	0.482 \pm 0.011 (+2.2)
QAT	GAT	None	52.8 \pm 0.7	30.1 \pm 14.5	76.3 \pm 1.2	41.9 \pm 1.1	0.702 \pm 0.011
	GAT	GPF-plus	54.9 \pm 5.3	19.7 \pm 3.0	77.5 \pm 0.9	43.1 \pm 1.2	0.693 \pm 0.025
	GAT	GPF-LoRAP	66.8 \pm 1.6 (+14.0)	40.6 \pm 7.3 (+10.5)	78.2 \pm 1.1 (+1.9)	43.8 \pm 0.7 (+1.9)	0.685 \pm 0.016 (+1.7)
DQ	GAT	None	68.7 \pm 7.5	41.9 \pm 5.9	90.3 \pm 0.5	54.2 \pm 0.5	0.556 \pm 0.022
	GAT	GPF-plus	58.3 \pm 5.4	39.1 \pm 9.6	93.1 \pm 0.6	51.5 \pm 0.8	0.589 \pm 0.018
	GAT	GPF-LoRAP	72.5 \pm 2.3 (+3.8)	54.4 \pm 4.6 (+12.5)	94.0 \pm 0.6 (+3.7)	57.5 \pm 1.4 (+3.3)	0.508 \pm 0.023 (+4.8)
A^2Q	GAT	None	82.6 \pm 0.8	71.2 \pm 0.9	92.5 \pm 0.6	61.9 \pm 1.2	0.674 \pm 0.007
	GAT	GPF-plus	83.4 \pm 0.5	71.8 \pm 0.2	92.4 \pm 0.8	62.3 \pm 1.4	0.685 \pm 0.008
	GAT	GPF-LoRAP	83.6 \pm 0.6 (+1.0)	72.5 \pm 0.8 (+1.3)	93.1 \pm 0.7 (+0.6)	62.9 \pm 1.0 (+1.0)	0.628 \pm 0.010 (+4.6)

$\mathbf{P}^{(l)}$ into two high-precision low rank matrices, $\mathbf{P}_A^{(l)} \in \mathbb{R}^{k \times r}$ and $\mathbf{P}_B^{(l)} \in \mathbb{R}^{r \times d}$, where the rank $r \ll \min(k, d)$. Then the prompts bases can be represented as the multiplication of these two low rank matrices, *i.e.*, $\mathbf{P}^{(l)} = \mathbf{P}_A^{(l)} \mathbf{P}_B^{(l)}$. This in turn reduces the number of parameters from $L \times k \times d$ to $L \times r \times (k + d)$. Given the quantized matrix of aggregated features $\mathbf{S}_q^{(l)}$, we then incorporate our input-dependent low-rank prompts into the l -th GNN layer as

$$\hat{\mathbf{S}}^{(l)} = DQ(\mathbf{S}_q^{(l)}) \quad (9)$$

$$\mathbf{P}_s^{(l)} = \text{Softmax}(\phi(\hat{\mathbf{S}}^{(l)})) \mathbf{P}_A^{(l)} \mathbf{P}_B^{(l)} \quad (10)$$

$$\mathbf{S}_q^{(l)*} = Q(\hat{\mathbf{S}}^{(l)} + \mathbf{P}_s^{(l)}), \quad (11)$$

where DQ is the *dequantization operator* (see Appendix A.1). Finally, the obtained prompted aggregation feature $\mathbf{S}_q^{(l)*}$ is used for further low-precision operations. By doing so, the gradient flows through the quantized weights to the full-precision prompts during the optimization process, allowing the learned prompt to be aware of the quantization effects. This awareness allows the model, when making pre-

dictions, to adapt its behavior to compensate for the low-bit representation, potentially leading to improved performance.

4.3 QAT frameworks & LoRAP integration

In order to make aggregation prompting applicable to any graph QAT framework (see the Appendix A.1 for an overview of QAT frameworks and other related work), we do not introduce any extra loss terms. Instead, we optimize the prompt vectors together with the original quantized model parameters under the framework existing objective function. We also deliberately avoid freezing the quantized GNN weights. Unlike LLMs, GNNs typically contain far fewer parameters, so the marginal computational overhead of jointly updating both prompts and network weights remains negligible. Therefore, if \mathbf{W} denotes the weights of the GNN and L_D is the framework existing loss, our task objective is $\arg \min_{Q, \mathbf{P}, \mathbf{W}} L_D$.

4.4 LoRAP kernel

Although in theory the low-rank structure of our prompting strategy introduces a negligible computational cost, executing it as a series of sequential operations incurs a notable latency overhead, totaling 93.5 μ s as illustrated in Fig. 4. For such

lightweight projections (e.g., GEMMs) and element-wise additions, the bottleneck shifts from computation to memory access, as intermediate activations must be repeatedly loaded from and stored to DRAM. To address this, we propose to fuse the LoRAP kernel using Triton [Tillet *et al.*, 2019], a Python-based GPU programming framework. By fusing the low-rank prompt generation and the residual addition directly into the aggregation operation, the LoRAP kernel allows intermediate states to be exchanged via the GPU register file or shared memory. This design eliminates redundant global memory accesses and kernel launch overheads, reducing the latency to $44.5\ \mu\text{s}$ (a $2.1\times$ speedup) and effectively rendering the prompt injection process more efficient.

5 Experiments

We integrate our prompt tuning strategy into 4 graph QAT frameworks to restore their performance under INT4 quantization bit-width, specifically standard QAT [Jacob *et al.*, 2018], Degree-Quant (DQ) [Tailor, 2020], A^2Q [Zhu *et al.*, 2023], and MixQ [Moustafa *et al.*, 2025]. The GNN architectures employed in our experiments include GIN [Xu *et al.*, 2018], GCN [Kipf and Welling, 2016], and GAT [Veličković *et al.*, 2017]. Evaluation results are reported across both node-level and graph-level tasks. For node-level tasks, the Cora and CiteSeer datasets are utilized, as well as large-scale OGB benchmarks (ogb-архив, ogb-products, and ogbn-mag) to verify scalability. For graph-level tasks, the REDDIT-BINARY, MNIST, CIFAR10, and ZINC datasets are adopted, where ZINC is specifically used for regression tasks. To provide a comparative baseline, we employ SOTA graph prompting methods, including GPF-plus, UniPrompt [Huang *et al.*, 2025], and EdgePrompt+ [Fu *et al.*, 2025a] for performance recovery of quantized GNNs. Detailed descriptions of the datasets are provided in the Appendix². Since GPF-plus and LoRAP can be seen as complementary approaches, our implementation integrates GPF-plus into the input feature space and LoRAP into the aggregation feature space, denoted as GPF-LoRAP. The additional hyperparameters introduced in our approach include the number of prompts (k) and the rank (r). For fair comparison, other hyperparameters retain the same configurations as those used in the original quantization frameworks, with only k and r subjected to tuning. Further implementation details are available in the Appendix.

5.1 Main results

We show how our prompt learning strategy improves the performance of 3 INT4 QAT frameworks in the Table 1. Full-precision (FP32) baselines are shown at the top. Under the naive QAT framework (INT4 QAT), all architectures suffer severe accuracy drops when no prompt is used (*e.g.*, for GIN, Cora accuracy falls from 77.6% to 44.2%). Introducing GPF-plus yields only a marginal recovery, whereas GPF-LoRAP consistently narrows this gap, improving GIN by $+0.9\% / +4.1\%$ on Cora/Citeseer, GCN by $+4.9\% / +0.5\%$, and

²Note that, to ensure a fair and correct comparison, we follow the same experimental setting (including datasets and model architectures) of the QAT frameworks our work is based on.

Table 2: Results for QAT & DQ GIN in INT4 & 8 on Reddit-Binary.

Quant. Frame.	Model	Prompt Method	REDDIT-BIN (Acc. %) \uparrow
QAT-W8A8	GIN	None	92.2 ± 2.3
		None	76.1 ± 7.5
		GPF-plus	72.2 ± 3.7
DQ-W8A8	GIN	GPF-LoRAP	81.2 ± 2.7 (+5.1)
		None	91.8 ± 2.3
		GPF-plus	94.1 ± 2.0
QAT-W4A4	GIN	GPF-LoRAP	94.6 ± 2.7 (+2.8)
		None	52.4 ± 5.8
		GPF-plus	53.8 ± 5.7
DQ-W4A4	GIN	GPF-LoRAP	69.6 ± 5.6 (+17.2)
		None	89.4 ± 2.9
		GPF-plus	92.3 ± 2.4
		GPF-LoRAP	93.0 ± 3.1 (+3.6)

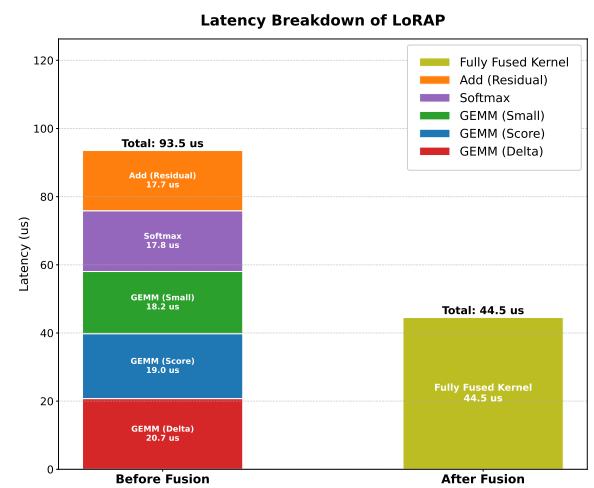


Figure 4: Latency comparison.

GAT by $+14.0\% / +10.5\%$, while also boosting graph classification ($+7.1\%$ for GIN on CIFAR-10). Under DQ, which already retains more of the original accuracy, GPF-LoRAP further boosts performance across the board, confirming its generality. Even with the A^2Q framework, which already narrows the FP32 gap, GPF-LoRAP delivers consistent improvements. Remarkably, when combined with the A^2Q quantization, GPF-LoRAP not only recovers nearly all of the performance lost to low-bit compression but actually surpasses the original FP32 baseline in several cases. For example, on Cora, GIN quantized with A^2Q and equipped with our prompts achieves 78.5% accuracy, outperforming the 77.6% of the full-precision mode. In summary, GPF-LoRAP outperforms both the unprompted baseline and the GPF-plus strategy, often halving the remaining accuracy gap with the FP32 model. The benefits are pronounced across nearly all settings, demonstrating that GPF-LoRAP can act as a general training strategy for GNN QAT frameworks.

Table 3: Ablation study for A2Q GIN on the MNIST dataset.

Config	Average bits	#Additional Parameters	MNIST (Acc. %)↑
FP32	32	0KB	96.4 ± 0.4
INT4	4	0KB	94.4 ± 0.2
+ GPF-plus	4	17.26KB	96.0 ± 0.5
+ GPF-plus + LoRAP (GPF-LoRAP)	4	26.95KB	96.2 ± 0.4
A2Q	3.75	0KB	95.7 ± 0.2
+ GPF-plus	3.75	17.26KB	95.9 ± 0.4
+ EdgePrompt+	3.78	103.44KB	95.5 ± 0.3
+ AP	3.78	43.03KB	95.9 ± 0.1
+ LoRAP	3.76	9.69KB	96.2 ± 0.3
+ GPF-plus + AP	3.78	60.29KB	96.3 ± 0.1
+ GPF-plus + LoRAP (GPF-LoRAP)	3.76	26.95KB	96.4 ± 0.2

Table 4: Performance comparison on large-scale datasets.

Task	Method	Acc	Bits
ogb-arxiv (GCN)	FP32	71.7 ± 0.3	32
	A2Q	71.1 ± 0.3	2.7
	+GPF-Plus	70.9 ± 0.3	2.7
	+UniPrompt	71.3 ± 0.4	2.7
	+LoRAP	73.6 ± 0.1	2.7
	MixQ	69.3 ± 0.0	7.1
	+GPF-Plus	70.1 ± 0.2	7.1
	+UniPrompt	69.4 ± 0.2	7.1
	+LoRAP	71.9 ± 0.1	7.0

5.2 Results on different bit widths

Table 2 presents the Reddit-Binary classification accuracy of GIN under different bit-widths, using both standard QAT and DQ, with three prompting strategies: (1) no prompts, (2) node prompting with GPF-plus, and (3) GPF-LoRAP. While standard GPF-plus is unstable and sometimes lowers the accuracy, GPF-LoRAP consistently improves performance. In QAT-W8A8, GPF-LoRAP pushes the accuracy beyond the full-precision limit in the stronger DQ-W8A8 setting. Moreover, in the aggressive INT4 regime, when the model fails completely, GPF-LoRAP provides a huge recovery (+17%). This shows that LoRAP can fix severe quantization errors.

5.3 Results on large-scale datasets

To verify the scalability of our approach, we extend our evaluation to large-scale benchmarks. As shown in Table 12, LoRAP consistently yields the highest accuracy across all quantization frameworks. Additional results on ogb-products and ogbn-mag, where ogbn-mag is inductive and heterogeneous, are included in the Appendix A.10.

5.4 Latency comparison

In Table 5, we report the latency for a single GCN layer on the CIFAR-10 dataset. The hardware for testing is an AMD

Table 5: Latency and Speedup comparison on CPU and GPU devices. Speedup is calculated relative to the FP32 baseline.

Device	Setting	Latency	Speedup
CPU	FP32	36.66ms	1.00×
	INT8	15.36ms	2.39×
	INT8+LoRAP	18.29ms	2.00×
	INT4	11.78ms	3.11×
	INT4+LoRAP	14.77ms	2.48×
GPU	FP32	0.69ms	1.00×
	INT8	0.43ms	1.60×
	INT8+LoRAP	0.52ms	1.33×
	INT8+LoRAP (fused)	0.48ms	1.44×
	INT4	0.33ms	2.09×
	INT4+LoRAP	0.42ms	1.64×
	INT4+LoRAP (fused)	0.37ms	1.86×

EPYC 9124 16-Core CPU paired with an Nvidia RTX4090 GPU. On the CPU, quantizing both weights and activations to 8 bits achieves a 2.39× speedup over the FP32 baseline. Incorporating the FP32 LoRAP prompt module on top of the W8A8 layer incurs minimal cost, still running almost 2.00× faster than the original FP32 layer. On the GPU, the efficiency is further improved by our fused kernel design. Specifically, the INT4+LoRAP (fused kernel) maintains a 1.86× speedup compared to the FP32 baseline, demonstrating that the overhead of prompt injection is effectively mitigated.

5.5 Ablation study

Table 3 presents an ablation study on the MNIST dataset using A^2Q -quantized GIN models to isolate the impact of different prompting strategies, including GPF-plus, EdgePrompt+, full-rank aggregation prompting (AP), and our proposed GPF-LoRAP. EdgePrompt+ degrades the performance despite incurring the highest parameter overhead. In contrast, the low-rank constraint in LoRAP demonstrates superior parameter efficiency by outperforming the full-rank AP strategy while requiring significantly fewer trainable parameters. Furthermore, there is a clear synergy between node and aggregation prompting: while GPF-plus and LoRAP individually improve over the baseline, their combination (GPF-LoRAP) yields the strongest gain, successfully bridging the gap to match the FP32 benchmark. In Appendix A.9, we provide further comparisons with other SOTA prompting methods.

6 Conclusion

We proposed the first integration of prompt learning in the context of QAT for GNNs. We introduced LoRAP, a low-rank aggregation prompting method, to compensate for the information loss incurred after quantization. Extensive experiments with multiple quantization frameworks and GNN architectures showed that LoRAP, when combined with GPF-plus, is able to recover the lost performance and, in several cases, surpasses the accuracy of full-precision models, all while adding minimal overhead. Our approach offers a novel and effective way to improve the performance of GNNs operating in a resource-constrained environment.

References

[Achanta *et al.*, 2012] R. Achanta, A. Shaji, K. Smith, A. Lucchi, P. Fua, and S. Süsstrunk. Slic superpixels compared to state-of-the-art superpixel methods. *IEEE Transactions on Pattern Analysis and Machine Intelligence*, 34(11):2274–2282, 2012.

[Bahng *et al.*, 2022] Hyojin Bahng, Ali Jahanian, Swami Sankaranarayanan, and Phillip Isola. Exploring visual prompts for adapting large-scale models. *arXiv preprint arXiv:2203.17274*, 2022.

[Brown *et al.*, 2020] Tom B. Brown, Benjamin Mann, Nick Ryder, Melanie Subbiah, Jared Kaplan, Prafulla Dhariwal, Arvind Neelakantan, Pranav Shyam, Girish Sastry, Amanda Askell, et al. Language models are few-shot learners. *arXiv preprint arXiv:2005.14165*, 2020.

[Chen *et al.*, 2025] Qin Chen, Liang Wang, Bo Zheng, and Guojie Song. Dagprompt: Pushing the limits of graph prompting with a distribution-aware graph prompt tuning approach. *arXiv preprint arXiv:2501.15142*, 2025.

[Dettmers *et al.*, 2022] Tim Dettmers, Mike Lewis, Younes Belkada, and Luke Zettlemoyer. Gpt3. int8 (): 8-bit matrix multiplication for transformers at scale. *Advances in neural information processing systems*, 35:30318–30332, 2022.

[Dettmers *et al.*, 2024] Tim Dettmers, Artidoro Pagnoni, Ari Holtzman, and Luke Zettlemoyer. Qlora: Efficient fine-tuning of quantized llms. *Advances in Neural Information Processing Systems*, 36, 2024.

[Esser *et al.*, 2020] Steven K Esser, Jeffrey L McKinstry, Deepika Bablani, Rathinakumar Appuswamy, and Dharmendra S Modha. Learned step size quantization. In *International Conference on Learning Representations*, 2020.

[Fang *et al.*, 2023] Taoran Fang, Yunchao Zhang, Yang Yang, Chunping Wang, and Lei Chen. Universal prompt tuning for graph neural networks. *Advances in Neural Information Processing Systems*, 36:52464–52489, 2023.

[Fang *et al.*, 2024] Taoran Fang, Yunchao Zhang, Yang Yang, Chunping Wang, and Lei Chen. Universal prompt tuning for graph neural networks. *Advances in Neural Information Processing Systems*, 36, 2024.

[Feng *et al.*, 2020] Boyuan Feng, Yuke Wang, Xu Li, Shu Yang, Xueqiao Peng, and Yufei Ding. Sqquant: Squeezing the last bit on graph neural networks with specialized quantization. In *2020 IEEE 32nd international conference on tools with artificial intelligence (ICTAI)*, pages 1044–1052. IEEE, 2020.

[Fey and Lenssen, 2019] Matthias Fey and Jan Eric Lenssen. Fast graph representation learning with pytorch geometric, 2019.

[Fu *et al.*, 2025a] Xingbo Fu, Yinhuan He, and Jundong Li. Edge prompt tuning for graph neural networks. In *The Thirteenth International Conference on Learning Representations*, 2025.

[Fu *et al.*, 2025b] Xingbo Fu, Yinhuan He, and Jundong Li. Edge prompt tuning for graph neural networks. *arXiv preprint arXiv:2503.00750*, 2025.

[Hetzl *et al.*, 2021] Leon Hetzel, David S Fischer, Stephan Günemann, and Fabian J Theis. Graph representation learning for single-cell biology. *Current Opinion in Systems Biology*, 28:100347, 2021.

[Huang *et al.*, 2025] Yongqi Huang, Jitao Zhao, Dongxiao He, Xiaobao Wang, Yawen Li, Yuxiao Huang, Di Jin, and Zhiyong Feng. One prompt fits all: Universal graph adaptation for pretrained models. In *The Thirty-ninth Annual Conference on Neural Information Processing Systems*, 2025.

[Hubara *et al.*, 2016] Itay Hubara, Matthieu Courbariaux, Daniel Soudry, Ran El-Yaniv, and Yoshua Bengio. Quantized neural networks: Training neural networks with low precision weights and activations. *arXiv preprint arXiv:1609.07061*, 2016.

[Jacob *et al.*, 2018] Benoit Jacob, Skirmantas Kligys, Bo Chen, Menglong Zhu, Matthew Tang, Andrew Howard, Hartwig Adam, and Dmitry Kalenichenko. Quantization and training of neural networks for efficient integer-arithmetic-only inference. In *Proceedings of the IEEE conference on computer vision and pattern recognition*, pages 2704–2713, 2018.

[Jia *et al.*, 2022] Menglin Jia, Luming Tang, Bor-Chun Chen, Claire Cardie, Serge Belongie, Bharath Hariharan, and Ser-Nam Lim. Visual prompt tuning. In *European conference on computer vision*, pages 709–727. Springer, 2022.

[Jin *et al.*, 2018] Wengong Jin, Regina Barzilay, and Tommi Jaakkola. Junction tree variational autoencoder for molecular graph generation, 2018.

[Kipf and Welling, 2016] Thomas N Kipf and Max Welling. Semi-supervised classification with graph convolutional networks. *arXiv preprint arXiv:1609.02907*, 2016.

[Kipf and Welling, 2017] Thomas N. Kipf and Max Welling. Semi-supervised classification with graph convolutional networks. In *5th International Conference on Learning Representations, ICLR 2017, Toulon, France, April 24-26, 2017, Conference Track Proceedings*. OpenReview.net, 2017.

[Kumar and Patel, 2023] Raj Kumar and Anil Patel. Challenges in low-bit quantization of graph neural networks. *ResearchGate Preprint*, 2023.

[Lester *et al.*, 2021] Brian Lester, Rami Al-Rfou, and Noah Constant. The power of scale for parameter-efficient prompt tuning. In *Proceedings of the 2021 Conference on Empirical Methods in Natural Language Processing*, 2021.

[Li and Liang, 2021] Xiang Lisa Li and Percy Liang. Prefix-tuning: Optimizing continuous prompts for generation. In *Proceedings of the 2021 Annual Meeting of the Association for Computational Linguistics*, 2021.

[Li and others, 2024] S. Li et al. Graphlora: Structure-aware contrastive low-rank adaptation for cross-graph transfer learning. *arXiv preprint arXiv:2409.16670*, 2024.

[Li et al., 2023] Zhikai Li, Xiaoxuan Liu, Banghua Zhu, Zhen Dong, Qingyi Gu, and Kurt Keutzer. Qft: Quantized full-parameter tuning of llms with affordable resources. *arXiv preprint arXiv:2310.07147*, 2023.

[Li et al., 2024a] Cheng Li, Hao Wang, and John Smith. Quantization methods for graph neural networks: A comprehensive survey. *Machines*, 12(5):345, 2024.

[Li et al., 2024b] Muyang Li, Yujun Lin, Zhekai Zhang, Tianle Cai, Xiuyu Li, Junxian Guo, Enze Xie, Chenlin Meng, Jun-Yan Zhu, and Song Han. Svdquant: Absorbing outliers by low-rank component for 4-bit diffusion models. In *The Thirteenth International Conference on Learning Representations*, 2024.

[Liu and Rossi, 2025] Chenyu Liu and Luca Rossi. Phgnn: A novel prompted hypergraph neural network to diagnose alzheimer’s disease. *arXiv preprint arXiv:2503.14577*, 2025.

[Liu et al., 2021] Xiaodong Liu, Yichao Zhang, Zhichao Ling, Yichun Guo, Tong Han, Yaru Guo, Maosong Sun, and Xiaoqiang Cui. P-tuning: Prompt tuning can be comparable to fine-tuning across scales and tasks. In *Proceedings of the 2021 Annual Meeting of the Association for Computational Linguistics*, 2021.

[Liu et al., 2022] Xiaodong Liu, Hongliang Peng, Yichao Zhang, Yiran Wei, and Maosong Sun. P-tuning v2: Prompt tuning can be comparable to fine-tuning at scale. In *Advances in Neural Information Processing Systems*, volume 35, 2022.

[Minello et al., 2025] Giorgia Minello, Alessandro Bicciato, Luca Rossi, Andrea Torsello, and Luca Cosmo. Graph generation via spectral diffusion. In *The Thirteenth International Conference on Learning Representations*, 2025.

[Moustafa et al., 2025] Samir Moustafa, Nils Kriege, and Wilfried N Gansterer. Efficient mixed precision quantization in graph neural networks. In *2025 IEEE 41st International Conference on Data Engineering (ICDE)*, pages 4038–4052. IEEE, 2025.

[Nagel et al., 2020] Markus Nagel, Rana Ali Amjad, Mart van Baalen, Christos Louizos, and Tijmen Blankevoort. Up or down? adaptive rounding for post-training quantization. In *International Conference on Learning Representations (ICLR)*, 2020.

[Rahmani et al., 2023] Saeed Rahmani, Asiyeh Baghbani, Nizar Bouguila, and Zachary Patterson. Graph neural networks for intelligent transportation systems: A survey. *IEEE Transactions on Intelligent Transportation Systems*, 24(8):8846–8885, 2023.

[Reiser et al., 2022] Patrick Reiser, Marlen Neubert, André Eberhard, Luca Torresi, Chen Zhou, Chen Shao, Houssam Metni, Clint van Hoesel, Henrik Schopmans, Timo Sommer, et al. Graph neural networks for materials science and chemistry. *Communications Materials*, 3(1):93, 2022.

[Tailor, 2020] Tailor. Degree-quant: Quantization-aware training for graph neural networks. *arXiv preprint arXiv:2008.05000*, 2020.

[Tang and Liu, 2010] Lei Tang and Huan Liu. Graph mining applications to social network analysis. *Managing and mining graph data*, pages 487–513, 2010.

[Tillet et al., 2019] Philippe Tillet, Hsiang-Tsung Kung, and David Cox. Triton: an intermediate language and compiler for tiled neural network computations. In *Proceedings of the 3rd ACM SIGPLAN International Workshop on Machine Learning and Programming Languages*, pages 10–19, 2019.

[Veličković et al., 2017] Petar Veličković, Guillem Cucurull, Arantxa Casanova, Adriana Romero, Pietro Lio, and Yoshua Bengio. Graph attention networks. *arXiv preprint arXiv:1710.10903*, 2017.

[Wang et al., 2025] Qunzhong Wang, Xiangguo Sun, and Hong Cheng. Does graph prompt work? a data operation perspective with theoretical analysis. In *ICML*, 2025.

[Wu et al., 2022] Shiwen Wu, Fei Sun, Wentao Zhang, Xu Xie, and Bin Cui. Graph neural networks in recommender systems: a survey. *ACM Computing Surveys*, 55(5):1–37, 2022.

[Xu et al., 2018] Keyulu Xu, Weihua Hu, Jure Leskovec, and Stefanie Jegelka. How powerful are graph neural networks? *arXiv preprint arXiv:1810.00826*, 2018.

[Xu et al., 2024] Zhaozhuo Xu, Zirui Liu, Beidi Chen, Shaochen Zhong, Yuxin Tang, Jue Wang, Kaixiong Zhou, Xia Hu, and Anshumali Shrivastava. Soft prompt recovers compressed llms, transferably. In *Forty-first International Conference on Machine Learning*, 2024.

[Zhu et al., 2023] Zeyu Zhu, Fanrong Li, Zitao Mo, Qinghao Hu, Gang Li, Zejian Liu, Xiaoyao Liang, and Jian Cheng. Aggregation-aware quantization for graph neural networks. *arXiv preprint arXiv:2302.00193*, 2023.

Appendices

A Appendix

A.1 Background and Related Work

Quantization Process.

Given a real-valued tensor x and bit-width b , we define the *quantization operator* $Q(\cdot)$ and *dequantization operator* $DQ(\cdot)$ as

$$Q(x) = \text{clip}\left(\text{round}\left(\frac{x}{S}\right) + Z, q_{\min}, q_{\max}\right) \quad (12)$$

$$DQ(x_q) = S(x_q - Z), \quad (13)$$

where the scale S and zero-point Z are computed as

$$S = \frac{x_{\max} - x_{\min}}{q_{\max} - q_{\min}}, \quad Z = \text{round}\left(\frac{-x_{\min}}{S}\right),$$

and the integer quantization bounds are

$$q_{\min} = 0, \quad q_{\max} = 2^b - 1 \quad (\text{unsigned}),$$

or

$$q_{\min} = -2^{b-1}, \quad q_{\max} = 2^{b-1} - 1 \quad (\text{signed}).$$

Here, x_{\min} and x_{\max} denote the minimum and maximum values of x . The function $\text{round}(\cdot)$ maps its argument to the nearest integer, and $\text{clip}(\cdot, q_{\min}, q_{\max})$ truncates values outside $[q_{\min}, q_{\max}]$ to the nearest bound. During inference, each real value x is quantized to $x_q = Q(x)$ and then dequantized back to $\hat{x} = DQ(x_q)$ for low-bitwidth storage and arithmetic.

Quantization Techniques.

Quantization is a key strategy for reducing the memory footprint and computational cost of deep neural networks by representing weights and activations with lower-precision numbers. Early work showed that 16-bit fixed-point quantization can be applied to training and inference with minimal accuracy loss and was later extended to 8-bit and sub-8-bit precisions [Jacob *et al.*, 2018]. Broadly speaking, these methods fall into two categories:

- **Post-Training Quantization (PTQ).** PTQ methods perform a lightweight calibration step on a pretrained full-precision model to determine optimal quantization parameters (namely scale, zero-point, and rounding directions) using only a small calibration dataset. A simple min–max calibration maps the observed activation range to integer bounds, while histogram-based techniques clip outliers by optimizing for minimal information loss according to percentile criteria [Nagel *et al.*, 2020].
- **Quantization-Aware Training (QAT).** QAT injects fake-quantization operations into both forward and backward passes so that the network learns to adapt its weights to low-precision representations. Early QAT works on binary and ternary networks demonstrated the feasibility of end-to-end gradient updates under discrete constraints [Hubara *et al.*, 2016]. Later methods introduced learnable scale and zero-point parameters [Jacob *et al.*, 2018], while Learned Step Size Quantization (LSQ) makes the quantization grid itself trainable for optimal precision–range trade-offs [Esser *et al.*, 2020]. Unlike PTQ, QAT updates both weights and quantization parameters during training, yielding higher accuracy, especially at very low bit-widths, at the cost of significantly longer training times.

Prompt Tuning.

Prompt tuning has emerged as a highly parameter-efficient strategy for adapting large pretrained models to downstream tasks by learning a small set of continuous prompt vectors, while keeping the original model weights frozen. Early work on in-context learning with discrete prompts demonstrated the power of prompting for few-shot tasks [Brown *et al.*, 2020]. Building on this idea, Lester *et al.* [Lester *et al.*, 2021] introduced *Prompt Tuning*, in which soft prompt embeddings are prepended to the input and optimized via gradient descent, achieving performance competitive with full fine-tuning using orders of magnitude fewer trainable parameters. Li and Liang [Li and Liang, 2021] further generalized this to *Prefix Tuning*, where trainable vectors are injected at every layer of a transformer. Liu *et al.* [Liu *et al.*, 2021; Liu *et al.*, 2022] proposed *P-Tuning* and *P-Tuning v2*, which scale soft prompting to very large language models by optimizing continuous prompts at multiple layers. In the vision domain, Visual Prompt Tuning (VPT) [Jia *et al.*, 2022] applies a similar soft-prompt mechanism to vision transformers. Despite these advances in natural language processing and computer vision, prompt tuning has been largely unexplored for graph-based models. Our work is the first to explore the use of prompt tuning for GNNs QAT.

Graph Prompting.

Inspired by the success of prompt learning in Natural Language Processing (NLP), graph prompting has emerged as a paradigm to bridge the gap between pre-training and downstream tasks by modifying the input graph rather than fine-tuning the entire model parameters. Early works focused on input-space adaptation: GPF and GPF-Plus [Fang *et al.*, 2024] introduce learnable vectors to node features. More recently, unified frameworks like UniPrompt [Huang *et al.*, 2025] and EdgePrompt [Fu *et al.*, 2025b] have attempted to optimize feature and structure prompts simultaneously. Theoretical understanding of this paradigm has also deepened; Wang *et al.* [Wang *et al.*, 2025] analyzed graph prompting from a data operation perspective, providing rigorous error bounds and proving that prompts essentially simulate graph transformation operators to align upstream and downstream tasks. Furthermore, to address distribution shifts in complex scenarios such as heterophilic graphs, DAGPrompT [Chen *et al.*, 2025] proposes a distribution-aware tuning framework that customizes prompts for hop-specific node requirements, significantly pushing the limits of prompting effectiveness.

Parameter-Efficient Fine-Tuning and LoRA on Graphs.

Parallel to prompting, Low-Rank Adaptation (LoRA) has gained traction for efficient model adaptation. In the graph domain, GraphLoRA [Li and others, 2024] applies LoRA to GNN weights combined with contrastive learning to enable efficient cross-graph transfer learning without catastrophic forgetting. Similarly, the GLoRA module within DAGPrompT [Chen *et al.*, 2025] utilizes low-rank adaptation to optimize the GNN encoder’s projection matrices for better distribution alignment. *Difference from our work:* It is crucial to distinguish our proposed LoRAP from these approaches. While GraphLoRA and DAGPrompT employ LoRA to adapt the *model backbone weights* for transfer learning tasks, our method applies a low-rank constraint specifically to the *aggregation prompt* injected into the message-passing stream. To the best of our knowledge, our work is the first to leverage low-rank prompting specifically as a compensation mechanism for *Quantization-Aware Training (QAT)*, utilizing the low-rank structure not just for parameter efficiency, but to regularize the quantization noise inherent in low-bit aggregation.

Quantization in GNNs.

Graph Neural Network (GNN) quantization has recently attracted attention as a means to reduce model size and accelerate inference on graph data [Li *et al.*, 2024a]. Unlike CNNs, GNNs pose unique challenges for quantization. Most notably, the irregular graph topology leads to highly variable node activation magnitudes (due to differing neighbor counts), making naive, uniform low-bit quantization prone to severe accuracy loss [Kumar and Patel, 2023]. Early attempts to apply standard 8-bit quantization to GNNs often resulted in drastic performance degradation at lower bit-widths [Kumar and Patel, 2023]. To address these issues, researchers have developed degree-aware, adaptive-precision, and other specialized quantization frameworks that explicitly leverage graph structure. Below, we summarize key approaches and their innovations in the context of GNN quantization.

Recent advances in GNN quantization emphasize leveraging graph structure to guide precision allocation. Degree-Quant (DQ) [Tailor, 2020] introduces a stochastic masking scheme during QAT that “protects” high-degree nodes in full precision and employs percentile-based clipping to determine optimal scale ranges, enabling both 4-bit and 8-bit models to nearly match full-precision accuracy. A²Q [Zhu *et al.*, 2023] further augments this idea by learning a mixed-precision assignment for each node according to its aggregation complexity: low-degree nodes use very few bits, while high-degree “hub” nodes receive higher bit-width. Continuous proxies and gradient-friendly approximations allow per-node bit optimization. In conclusion, these graph-aware and adaptive quantization strategies deliver efficient yet high-accuracy GNNs suitable for both large-scale and edge deployments.

A.2 Theoretical Analysis

To conduct a formal analysis, we first define some key terms:

- Let $X \in \mathbb{R}^{N \times D}$ be the full-precision (FP32) node feature matrix, where N is the number of nodes and D is the feature dimension.
- Let $A \in \mathbb{R}^{N \times N}$ be the (normalized) adjacency matrix, representing the graph’s topology.
- A simplified GNN layer can be represented by the aggregated feature matrix $M = f(X, A)$, and we omit the update phase $f()$ for simplification denoted as $M = AX$.
- The quantization function is $Q(\cdot)$, which maps a full-precision tensor to a low-precision tensor. The quantization process introduces an additive error ϵ , so the quantized feature matrix is $X_q = Q(X) = X + \epsilon_X$.
- The learnable prompt matrix is $P \in \mathbb{R}^{N \times D}$, where we set independent prompts for each nodes for illustration purpose.
- The ideal (full-precision) aggregated message is $M_{fp} = AX$.
- Our optimization objective is to learn a prompt P that minimizes the difference between the prompt-corrected quantized feature and the ideal feature. The loss function can be defined as: $\mathcal{L}(P) = \|M_{prompted,q} - M_{fp}\|_F^2$, where $\|\cdot\|_F$ is the Frobenius norm.

Theorem 1 (Optimization Decoupling)

In post-aggregation prompting ($AX_q + P$), the optimal prompt P_{post}^* directly compensates for the propagated quantization error $A\epsilon_X$ and its learning objective is decoupled from the graph aggregation operator A . In contrast, in pre-aggregation prompting ($A(X_q + P)$), the learning objective for the optimal prompt P_{pre}^* is deeply coupled with A , requiring the model to learn a complex, topology-dependent “pre-inverse” transformation.

Proof.

1. Analysis of the optimization problem for post-aggregation prompting ($M_{post} = AX_q + P$).

The loss function is

$$\mathcal{L}_{post}(P) = \|(AX_q + P) - AX\|_F^2.$$

Substitute $X_q = X + \epsilon_X$ to obtain

$$\mathcal{L}_{post}(P) = \|(A(X + \epsilon_X) + P) - AX\|_F^2 = \|(AX + A\epsilon_X + P) - AX\|_F^2 = \|A\epsilon_X + P\|_F^2.$$

To minimize this loss, the optimal solution is obtained when $A\epsilon_X + P = 0$, which means

$$P_{post}^* = -A\epsilon_X.$$

This result shows that the post-aggregation prompt P directly learn the additive inverse of the already propagated and amplified quantization error $A\epsilon_X$. We can also get the gradient of the loss function with respect to P as

$$\nabla_P \mathcal{L}_{post}(P) = 2(A\epsilon_X + P).$$

The optimization process is decoupled from the aggregation operator A itself; the task of P is to repair the *output* of the A operation, not to alter its *input*.

2. Analysis of the optimization problem for pre-aggregation prompting ($M_{pre} = A(X_q + P)$).

The loss function is

$$\mathcal{L}_{pre}(P) = \|A(X_q + P) - AX\|_F^2.$$

Substitute $X_q = X + \epsilon_X$ to obtain

$$\mathcal{L}_{pre}(P) = \|A(X + \epsilon_X + P) - AX\|_F^2 = \|(AX + A(\epsilon_X + P)) - AX\|_F^2 = \|A(\epsilon_X + P)\|_F^2.$$

To minimize this loss, we ideally need $A(\epsilon_X + P) = 0$. This means that $(\epsilon_X + P)$ must lie in the null space of A . This optimization objective is far more indirect. The prompt P must learn a signal that is the opposite of the original quantization error ϵ_X while also ensuring that their sum, $\epsilon_X + P$, results in zero after being processed by the operator A . Similarly, we can get the gradient of the loss function with respect to P is $\nabla_P \mathcal{L}_{pre}(P) = 2A^T A(\epsilon_X + P)$.

Here, the gradient signal is modulated by the matrix $A^T A$ (a matrix closely related to the graph Laplacian). This means that an update to any node’s prompt in P is influenced by the graph structure within its 2-hop neighborhood. The model must not only learn the inverse of the error but also consider the effect that the graph operator A will have during the learning process. This is a coupled and more difficult optimization problem because the prompts P itself must pass through the same aggregation process which will introduce and amplify the error.

By comparing the optimization objectives and gradient flows of the two methods, Theorem 1 is proven. Post-aggregation prompting decouples the error correction task from the graph aggregation, providing a more direct and stable optimization path.

Theorem 2 (Targeted Correction Capability)

In GNN quantization, systematic bias caused by high-in-degree nodes is a primary source of error. Post-aggregation prompting ($AX_q + P$) can directly and specifically correct the systematic bias in the aggregated message of node i by learning a node-specific row vector P_i . In contrast, pre-aggregation prompting ($A(X_q + P)$) cannot achieve such targeted correction because the prompt vector P_i for node i primarily affects the aggregated messages of its neighbors, not its own.

Proof.

For any node i , its aggregated message is the weighted sum of its neighbors’ features, i.e.,

$$M_i = \sum_{j \in \mathcal{N}(i)} A_{ij} X_j.$$

After quantization, the error in the aggregated message is

$$(A\epsilon_X)_i = \sum_{j \in \mathcal{N}(i)} A_{ij} \epsilon_{X,j}.$$

For a high-in-degree node with degree d_i , this sum contains a large number of error terms. The variance of this error and its potential systematic bias, $b_i = E[(A\epsilon_X)_i]$, will increase significantly.

1. Analysis of the correction mechanism of post-aggregation prompting.

The corrected message for node i is

$$(M_{post})_i = (AX_q)_i + P_i.$$

The error between the corrected message and the ideal message is

$$Error_i = (M_{post})_i - (M_{fp})_i = ((AX)_i + (A\epsilon_X)_i) + P_i - (AX)_i = (A\epsilon_X)_i + P_i.$$

To eliminate the systematic bias b_i , the model needs to learn P_i such that $E[Error_i] = 0$, which implies:

$$E[(A\epsilon_X)_i] + P_i = 0 \implies P_i = -b_i.$$

This mechanism is *targeted*. The i -th row vector of the prompt, P_i , acts directly on the final aggregated message of the i -th node. If the aggregated message for a high-in-degree node i has a systematic positive bias, the model can precisely cancel it by learning a corresponding negative P_i .

2. Analysis of the correction mechanism of pre-aggregation prompting.

The corrected message for node i is

$$(M_{pre})_i = (A(X_q + P))_i = \sum_{j \in \mathcal{N}(i)} A_{ij}(X_{q,j} + P_j).$$

The error between the corrected message and the ideal message is

$$\begin{aligned} Error_i &= (M_{pre})_i - (M_{fp})_i = \sum_{j \in \mathcal{N}(i)} A_{ij}(X_{q,j} + P_j) - \sum_{j \in \mathcal{N}(i)} A_{ij}X_j \\ &= \left(\sum_{j \in \mathcal{N}(i)} A_{ij}\epsilon_{X,j} \right) + \left(\sum_{j \in \mathcal{N}(i)} A_{ij}P_j \right) = (A\epsilon_X)_i + (AP)_i. \end{aligned}$$

To eliminate the systematic bias b_i , the model needs to adjust the prompt P such that $E[Error_i] = 0$, which implies

$$E[(A\epsilon_X)_i] + \sum_{j \in \mathcal{N}(i)} A_{ij}P_j = 0 \implies \sum_{j \in \mathcal{N}(i)} A_{ij}P_j = -b_i.$$

This mechanism is *non-targeted*. To correct the bias b_i for node i , the model must adjust the prompt vectors P_j of all its neighboring nodes. This creates a complex credit assignment problem: when node i 's message is corrupted by quantization, the gradient signal must be backpropagated to the prompts P_j of all its neighbors, but it is difficult to determine which neighbor's prompt should be responsible for the correction. For a high-in-degree node, this means coordinate adjusting hundreds or thousands of other nodes' prompt vectors, which is an extremely difficult learning task.

By analyzing the path of the correction signal (graph prompts), Theorem 2 is proven.

Theorem 3 (Non-emptiness of the ϵ -extended Bridge Set for Prompted Quantized GNNs)

Let F_{fp} be a pre-trained full-precision GNN model with weights W_{fp} , and let F_{θ^*} be its quantized counterpart with weights W_q . Let G be a given full-precision graph, and let $C(G) = F_{fp}(G)$ be the optimal embedding vector from the full-precision model. Let G_p denote a prompted quantized graph, constructed by applying a learnable prompt P from a prompt space \mathcal{P} to the quantized version of G . Let ϵ_{min} be the minimum achievable approximation error, defined as the minimum of the error function over all possible prompts, i.e.,

$$\epsilon_{min} = \min_{P \in \mathcal{P}} \|F_{\theta^*}(G_p(P)) - C(G)\|. \quad (14)$$

For any chosen error tolerance ϵ^* such that $\epsilon^* \geq \epsilon_{min}$, the ϵ -extended Bridge Set $\epsilon\text{-}B_G$ is non-empty. That is,

$$\epsilon\text{-}B_G = \{G_p \mid \|F_{\theta^*}(G_p) - C(G)\| \leq \epsilon^*\} \neq \emptyset. \quad (15)$$

The upper bound of ϵ is determined by the singular values of the Quantization Error matrix \mathcal{E} , i.e.,

$$\epsilon = \min_{\text{rank}(P) \leq k} \|F_{\theta^*}(G_p(P)) - C(G)\|_F \leq \sqrt{\sum_{j=k+1}^{\min(N, D')} \sigma_j^2(\mathcal{E})}, \quad (16)$$

where $\mathcal{E} = W_q AX_q - W_{fp} AX$.

Proof.

First, we consider the strict ‘Bridge Graph’, defined as $B_G = \{G_p \mid F_{\theta^*}(G_p) = C(G)\}$. The foundational premise is the surjectivity of the operator F_θ onto the continuous vector space \mathbb{R}^F . This premise does not hold in the context of quantization. The quantized model F_{theta} , due to its use of finite-precision arithmetic, can only produce a finite and discrete subset of vectors in \mathbb{R}^F . Therefore, the condition of exact equality $F_{\theta^*}(G_p) = C(G)$ is generally not satisfiable. Then the strict bridge set $G_p \in B_G$ is likely an empty set (\emptyset).

To address this, we analyze the approximation error. We define an error function $\mathcal{L}(P)$ dependent on the choice of prompt P , i.e.,

$$\mathcal{L}(P) = \|F_{\theta^*}(G_p(P)) - C(G)\|. \quad (17)$$

As established previously, assuming the prompt space \mathcal{P} is a compact set and the function $\mathcal{L}(P)$ is continuous with respect to the parameters of P , the *Extreme Value Theorem* guarantees that this error function attains a minimum value on \mathcal{P} . We define this minimum achievable error as ϵ_{min} .

The existence of a minimum error ϵ_{min} implies the existence of an optimal prompt $P^* \in \mathcal{P}$ such that

$$\mathcal{L}(P^*) = \|F_{\theta^*}(G_p(P^*)) - C(G)\| = \epsilon_{min}. \quad (18)$$

Let us denote the prompted graph generated using this optimal prompt as $G_p^* = G_p(P^*)$, which is the prompted quantized graph that best approximates the full-precision output. Consider the definition of the ϵ -extended Bridge Set, $\epsilon\text{-}B_G$, for a given error boundary ϵ^* . A graph $G_p \in \epsilon\text{-}B_G$ if its approximation error is less than or equal to ϵ^* . For any $\epsilon^* \geq \epsilon$, the optimal prompted graph G_p^*

$$\|F_{\theta^*}(G_p^*) - C(G)\| = \epsilon \leq \epsilon^*. \quad (19)$$

Because we have found at least one element, G_p^* , that belongs to the set $\epsilon\text{-}B_G$ (for any $\epsilon^* \geq \epsilon$), we conclude that the set is non-empty. From Equation (17), we get

$$\mathcal{L}(P) = \|W_q(AX_q + P) - W_{fp}(AX)\|_F \quad (20)$$

$$= \|W_qAX_q + W_qP - W_{fp}AX\|_F \quad (21)$$

$$= \|(W_qAX_q - W_{fp}AX) + W_qP\|_F. \quad (22)$$

Let $\mathcal{E} = W_qAX_q - W_{fp}AX$. This term represents the total inherent error of the unprompted quantized model relative to the full-precision model. The optimization problem simplifies to:

$$\min_{\text{rank}(P) \leq k} \|\mathcal{E} + W_qP\|_F. \quad (23)$$

We define a new matrix $Q = -W_qP$. Since $\text{rank}(P) \leq k$, the matrix product W_qP also has a rank of at most k (i.e., $\text{rank}(Q) \leq k$). Minimizing the loss is equivalent to finding the best rank- k matrix Q that approximates the error \mathcal{E} in the output space:

$$\min_{\text{rank}(Q) \leq k} \|\mathcal{E} - Q\|_F. \quad (24)$$

According to the *Eckart-Young-Mirsky Theorem*, the optimal rank- k approximation Q^* for the error matrix \mathcal{E} is obtained via Truncated Singular Value Decomposition (SVD). Let the SVD of the error be

$$\mathcal{E} = U\Sigma V^T = \sum_{i=1}^R \sigma_i u_i v_i^T, \quad (25)$$

where $\sigma_1 \geq \sigma_2 \geq \dots \geq \sigma_R$ are the singular values. The optimal approximation Q^* captures the first k principal components (largest singular values). Consequently, the residual error ϵ consists of the remaining tail components

$$\epsilon = \sqrt{\sum_{i=k+1}^R \sigma_i^2(\mathcal{E})}. \quad (26)$$

The error is strictly determined by the sum of squares of the singular values of the hybrid error matrix starting from index $k+1$. Thus

$$\epsilon \leq \sqrt{\sum_{j=k+1}^{\min(N, D')} \sigma_j^2(W_qAX_q - W_{fp}AX)}. \quad (27)$$

This completes the proof.

Table 6: Overall statistics for the datasets used in this work.

Task	Name	Graphs	Nodes	Edges	Features	Classes
Node-level	Cora	1	2,708	10,556	1,433	7
	CiteSeer	1	3,327	9,104	3,703	6
	PubMed	1	19,717	88,648	500	3
	OGB-Arxiv	1	169,343	1,166,243	128	40
	OGB-Products	1	2,449,029	61,859,140	100	47
	OGB-Mag	1	1,939,743	25,582,108	128	349
Graph-level	REDDIT-BINARY	2000	~429.6	~995.5	0	2
	REDDIT-M	4999	~508.8	~549.9	0	5
	D&D	1178	~284.3	~715.6	89	2
	PROTEINS	1113	~39.1	~145.6	3	2
	IMDB-B	1000	~19.8	~193.1	0	2
	MNIST	70000	~71	~565	3	10
	CIFAR10	60000	~117.6	~941.2	5	10
	ZINC	12000	~23	~49.8	28	—

A.3 Datasets

Table 6 summarizes the key properties of all datasets considered in this paper. For node-level tasks, we utilize the standard citation networks Cora, CiteSeer, and PubMed, in which each node represents a document and each edge a citation link. To verify scalability, we also incorporate large-scale OGB benchmarks, including OGB-Arxiv, OGB-Products, and the heterogeneous OGB-Mag. In these datasets, node features are primarily bag-of-words vectors or pretrained features, and the task is to predict the class in a semi-supervised setting [Kipf and Welling, 2017]. Regarding graph-level tasks, MNIST and CIFAR-10 are image-classification datasets converted into superpixel graphs using SLIC, so that nodes correspond to perceptually similar pixel clusters [Achanta *et al.*, 2012]. ZINC consists of molecular graphs with atoms as nodes and bonds as edges for regression tasks [Jin *et al.*, 2018], while D&D and PROTEINS are included as bioinformatics benchmarks for protein classification. Finally, REDDIT-BINARY, REDDIT-M, and IMDB-B comprise social network graphs. The REDDIT datasets are extracted from Reddit threads where an edge denotes an interaction between two users, while IMDB-B captures actor collaborations. We evaluate the graph classification performance using 10-fold cross validation. We employ the standard train/validation/test splits for MNIST, CIFAR-10, ZINC, and OGB datasets, while we adopt the semi-supervised split from [Kipf and Welling, 2017] for citation networks, and we report the average accuracy over the folds for the TUDatasets (REDDIT, D&D, PROTEINS, IMDB-B).

A.4 Experimental Setup

To ensure a fair comparison, we replicate the GNN architectures and FP32 baselines from DQ [Tailor, 2020] and A²Q [Zhu *et al.*, 2023] across all tasks. Table 7 details the specific configurations (number of layers, hidden-unit sizes, and the presence of skip connections) used in our experiments. We implement the QAT, DQ, and A²Q frameworks in PyTorch Geometric [Fey and Lenssen, 2019], adhering to the original hyperparameter settings of each method. All quantized models are trained with the Adam optimizer; the only parameters we vary are the number of prompts k , selected from $\{5, 10, 20, 40\}$, and the prompt rank r , chosen from $\{1, 2, 4, 8\}$. Results on Cora, CiteSeer, and ogb-axiv are averaged over 100 independent runs with different random seeds, while results on MNIST, CIFAR-10, and ZINC are averaged over 10 runs. For REDDIT-BINARY, we perform 10-fold cross-validation with a fixed split seed of 12345.

For the classification tasks (Cora, CiteSeer, MNIST, CIFAR-10, REDDIT-BINARY), we report the accuracy

$$\text{Accuracy} = \frac{1}{N} \sum_{i=1}^N \mathbf{1}(y_i = \hat{y}_i), \quad (28)$$

where y_i and \hat{y}_i are the true and predicted labels, respectively, and $\mathbf{1}(\cdot)$ is the indicator function.

For the regression task on ZINC, we use the Mean Absolute Error (MAE) loss

$$\text{MAE} = \frac{1}{N} \sum_{i=1}^N |y_i - \hat{y}_i|, \quad (29)$$

where y_i is the ground-truth property value and \hat{y}_i is the model prediction.

As for the experimental environment, all experiments were carried out on servers featuring an AMD EPYC 9124 16-core CPU paired with four NVIDIA RTX 4090 GPUs and running Ubuntu 22.04. Each node has 512 GB of RAM, and we used CUDA 12.7 with PyTorch 2.7.0 for all GPU-accelerated workloads.

Table 7: Architectural configurations on selected datasets.

Model	Property	Cora	CiteSeer	MNIST	CIFAR10	ZINC	REDDIT-BINARY
GCN	Layers	2	2	5+1 MLP	5+1 MLP	5+1 MLP	–
	Hidden units	16	16	146	146	145	–
	Skip connection	NO	NO	YES	YES	YES	–
GIN	Layers	2	2	5+1 MLP	5+1 MLP	5+1 MLP	5
	Hidden units	16	16	110	110	110	64
	Skip connection	NO	NO	YES	YES	YES	NO
GAT	Layers	2	2	5+1 MLP	5+1 MLP	5+1 MLP	–
	Hidden units	$8 \times h$	$8 \times h$	$19 \times h$	$19 \times h$	$18 \times h$	–
	Skip connection	NO	NO	YES	YES	YES	–

A.5 Discussion on the Integration between LoRAP and Quantization Methods

Here we discuss how LoRAP can be orthogonally integrated with weight compensation methods. We use SVDQuant [Li *et al.*, 2024b] as an example. Consider a linear transformation with input $\mathbf{X} \in \mathbb{R}^{b \times m}$ and weight matrix $\mathbf{W} \in \mathbb{R}^{m \times n}$, where b is the batch size and m, n are the input and output channel dimensions. We quantify the error introduced by the quantization as the Frobenius norm of the difference between the full-precision product and the product of their quantized counterparts, *i.e.*,

$$E(\mathbf{X}, \mathbf{W}) = \|\mathbf{X} \mathbf{W} - Q(\mathbf{X}) Q(\mathbf{W})\|_F. \quad (30)$$

The key idea of [Li *et al.*, 2024b] is to split the weight quantization problem into a low-rank component and a small residual. Concretely, they factorize the (possibly transformed) weight matrix as

$$\hat{\mathbf{W}} = \mathbf{L}_1 \mathbf{L}_2 + \mathbf{R},$$

where $\mathbf{L}_1 \in \mathbb{R}^{m \times r}$ and $\mathbf{L}_2 \in \mathbb{R}^{r \times n}$ are rank- r factors and \mathbf{R} captures the remaining residual. Here, $\hat{\mathbf{X}} = \mathbf{X} \text{diag}(\boldsymbol{\lambda})^{-1}$ denotes a smoothed version of \mathbf{X} , where each channel of the input is scaled by the inverse of its corresponding per-channel factor $\boldsymbol{\lambda} \in \mathbb{R}^m$, and the weight matrix \mathbf{W} is adjusted accordingly to preserve the correct output scale.

Thus, for an input $\hat{\mathbf{X}}$, the full-precision product can be written and approximated as

$$\hat{\mathbf{X}} \hat{\mathbf{W}} = \hat{\mathbf{X}} \mathbf{L}_1 \mathbf{L}_2 + \hat{\mathbf{X}} \mathbf{R} \approx \underbrace{\hat{\mathbf{X}} \mathbf{L}_1 \mathbf{L}_2}_{\substack{\text{16-bit} \\ \text{low-rank branch}}} + \underbrace{Q(\hat{\mathbf{X}}) Q(\mathbf{R})}_{\substack{\text{4-bit} \\ \text{residual branch}}}. \quad (31)$$

Accordingly, the resulting quantization error reduces to the residual term alone,

$$\|\hat{\mathbf{X}} \hat{\mathbf{W}} - (\hat{\mathbf{X}} \mathbf{L}_1 \mathbf{L}_2 + Q(\hat{\mathbf{X}}) Q(\mathbf{R}))\|_F = \|\hat{\mathbf{X}} \mathbf{R} - Q(\hat{\mathbf{X}}) Q(\mathbf{R})\|_F \quad (32)$$

$$\|\hat{\mathbf{X}} \mathbf{R} - Q(\hat{\mathbf{X}}) Q(\mathbf{R})\|_F = E(\hat{\mathbf{X}}, \mathbf{R}), \quad (33)$$

where $\mathbf{R} = \hat{\mathbf{W}} - \mathbf{L}_1 \mathbf{L}_2$.

Recall that LoRAP reduces the aggregation-quantization loss, *i.e.*,

$$\arg \min_{Q, \mathbf{P}} \|f(\mathbf{X}, \mathbf{A}) - (f(Q(\mathbf{X}), \mathbf{A}) + \mathbf{P})\|_F \approx 0. \quad (34)$$

Then, by using methods like SVDQuant, the layer-wise quantization error can also be reduced,

$$\|f(\mathbf{X}, \mathbf{A}) \mathbf{R} - (f(Q(\mathbf{X}), \mathbf{A}) + \mathbf{P}) Q(\mathbf{R})\|_F \quad (35)$$

$$\|f(\mathbf{X}, \mathbf{A}) \mathbf{R} - (f(Q(\mathbf{X}), \mathbf{A}) + \mathbf{P}) Q(\mathbf{R})\|_F = E(f(\mathbf{X}, \mathbf{A}), \mathbf{R}). \quad (36)$$

A.6 Impact of the Number of Prompts k and the Aggregation Rank r

Table 8 reports the mean loss of GPF-LoRAP using A²Q (INT4) and GIN on the ZINC dataset for different numbers of prompts k and aggregation rank r . For low ranks, as k increases from 5 to 40, the loss generally decreases: at $r = 1$ it drops from 0.382 to 0.368 and at $r = 2$ from 0.370 to the overall minimum of 0.361. For higher ranks ($r = 4$ and $r = 8$), the lowest losses occur at $k = 20$ (0.373 and 0.374, respectively) before slightly rising at $k = 40$. Overall, the best performance is achieved at $r = 2, k = 40$ with a mean loss of 0.361, confirming that moderate prompt counts and rank values yield the lowest prediction error. Overall, the optimal trade-off between prompt count and rank depends on the performance and computational budget.

Table 8: GPF-LoRAP with A^2Q (INT4) for GIN on ZINC, mean \pm std deviation for varying number of prompts k and rank r .

$r \setminus k$	5	10	20	40
1	0.382 ± 0.013	0.379 ± 0.011	0.378 ± 0.009	0.368 ± 0.012
2	0.370 ± 0.011	0.372 ± 0.005	0.372 ± 0.009	0.361 ± 0.010
4	0.378 ± 0.014	0.376 ± 0.017	0.373 ± 0.011	0.380 ± 0.014
8	0.380 ± 0.014	0.374 ± 0.015	0.374 ± 0.015	0.380 ± 0.011

Table 9: Training time for various quantization frameworks and prompting strategies on GIN (INT4).

Quant. Framework	Accuracy	Training Time
QAT	52.4 ± 5.8	74.67s
QAT-GPF-plus	53.8 ± 5.7	79.86s
QAT-GPF-LoRAP	69.6 ± 5.6	78.36s
DQ	89.4 ± 2.9	6398.54s
DQ-GPF-plus	92.3 ± 2.4	6446.86s
DQ-GPF-LoRAP	93.0 ± 3.1	6442.77s
A^2Q	89.2 ± 2.3	1040.29s
A^2Q -GPF-plus	89.6 ± 3.4	1063.73s
A^2Q -GPF-LoRAP	92.6 ± 2.5	1048.08s

A.7 Training Time Evaluation

Table 9 reports the average accuracy (mean \pm std deviation over 10 seeds) and total training time for each quantization framework on GIN (INT4), measured on a single Intel i5-14600KF CPU machine with 64GB RAM, one RTX 4090 GPU, and running Ubuntu 22.04. In the QAT setting, adding GPF-plus increases the training time from 74.67s to 79.86s, while GPF-LoRAP requires 78.36s. Under DQ, the baseline runtime of 6398.54s is only marginally affected by prompting: DQ-GPF and DQ-aggr take 6446.86s and 6442.77s, respectively. For A^2Q , GPF-plus adds 23.44s and GPF-LoRAP adds 7.79s to the 1040.29s baseline. These results confirm that GPF-plus and GPF-LoRAP introduce only minimal additional training cost across all quantization frameworks.

A.8 Impact of Different Aggregation Methods

We further evaluate the robustness of our method across different aggregation mechanisms, namely sum, mean, and max. As shown in Table 10, GPF-LoRAP consistently achieves the best performance across all settings. A key observation is that node prompting (GPF) exhibits instability depending on the aggregation type; specifically, it suffers a significant performance drop in the sum aggregation (decreasing from 77.4% to 72.7%). We hypothesize that adding prompts directly to node features can disrupt the magnitude of aggregated signals when simple summation is used. In contrast, by injecting prompts post-aggregation, GPF-LoRAP effectively corrects this distortion, not only recovering the loss but reaching a peak accuracy of 78.5%. Furthermore, GPF-LoRAP outperforms the baselines in both mean (78.7%) and max (77.9%) aggregations, demonstrating that our aggregation-aware strategy effectively generalizes to various message-passing dynamics.

A.9 Comparison with State-of-the-Art Prompting Methods

We further benchmark GPF-LoRAP against recent state-of-the-art graph prompting baselines, including UniPrompt and EdgePrompt, integrated into three distinct quantization frameworks: DQ, A^2Q , and MixQ. As presented in Table 11, GPF-LoRAP consistently outperforms all competing methods across both node and graph classification tasks. For instance, under the DQ framework on the Cora-GCN task, GPF-LoRAP achieves an accuracy of 78.0%, significantly surpassing UniPrompt (72.8%) and EdgePrompt (73.1%). A particularly striking improvement is observed on the Reddit-Binary dataset, where adding LoRAP

Table 10: Performance comparison with different aggregation functions.

Method \ Aggr	sum	mean	max
None	77.4 ± 0.9	76.9 ± 1.2	77.1 ± 0.6
GPF	72.7 ± 0.8	77.1 ± 0.9	77.3 ± 1.8
GPF-LoRAP	78.5 ± 1.0	78.7 ± 0.8	77.9 ± 1.1

Table 11: Comparison of accuracy and bit-width on node and graph classification tasks.

Method	Node Classification			Graph Classification		
	Task	Acc	Bits	Task	Acc	Bits
DQ	Cora-GCN	72.5 ± 3.7	4.0	Reddit-Binary	52.4 ± 5.8	4.0
+GPF-Plus		72.3 ± 2.8	4.0		53.8 ± 5.7	4.0
+UniPrompt		72.8 ± 2.4	4.0		-	-
+EdgePrompt+		73.1 ± 2.5	4.0		53.2 ± 4.9	4.0
+LoRAP		77.7 ± 1.8	4.0		70.1 ± 5.6	4.0
+GPF-LoRAP		78.0 ± 2.5	4.0		69.6 ± 5.6	4.0
A2Q	Cora-GCN	76.1 ± 0.3	1.7	MNIST	95.7 ± 0.2	3.8
+GPF-Plus		78.0 ± 0.1	1.7		95.9 ± 0.4	3.8
+UniPrompt		78.5 ± 0.2	1.7		-	-
+EdgePrompt+		75.9 ± 0.3	1.7		95.5 ± 0.3	3.8
+LoRAP		79.1 ± 0.1	1.7		96.2 ± 0.3	3.8
+GPF-LoRAP		79.1 ± 0.1	1.7		96.4 ± 0.2	3.8
MixQ	Cora-GCN	68.7 ± 2.7	3.8	Reddit-Binary	72.8 ± 3.5	5.9
+GPF-Plus		71.3 ± 1.8	3.8		72.5 ± 2.7	5.8
+UniPrompt		73.6 ± 2.6	3.9		-	-
+EdgePrompt+		71.2 ± 2.2	3.8		72.8 ± 3.1	5.8
+LoRAP		75.9 ± 1.6	3.8		75.6 ± 2.8	5.7
+GPF-LoRAP		76.5 ± 1.0	3.8		76.6 ± 3.4	5.7

to the DQ baseline boosts accuracy from 52.4% to 70.1%, demonstrating exceptional capability in recovering structural information lost during quantization. These results confirming that LoRAP serves as a robust and generalized plug-and-play module for enhancing various QAT strategies.

A.10 Results on Large-Scale Datasets

To verify the scalability of our approach, we extended our evaluation to three large-scale benchmarks: ogb-arxiv, ogb-products, and the heterogeneous graph ogbn-mag. As shown in Table 12, LoRAP consistently yields the highest accuracy across all tasks and quantization frameworks. A crucial observation is that standard node-level prompting method GPF-Plus struggle in these large-scale quantized settings. For instance, on the heterogeneous ogbn-mag dataset under the A2Q framework, applying GPF-Plus actually degrades the baseline performance from 32.7% to 30.4%. In contrast, LoRAP successfully mitigates these errors, boosting the accuracy to 34.2%. Similarly, on ogb-products, LoRAP improves the MixQ baseline by a solid margin (+2.5%), validating its robustness and effectiveness in handling diverse graph structures and scales.

A.11 Convergence Analysis of Joint Optimization

Finally, we analyze the convergence properties of the joint optimization objective, which simultaneously updates the discrete quantization parameters (Q), the continuous model weights (W), and the low-rank aggregation prompts (P). While standard QAT typically suffers from due to the non-differentiable nature of the straight-through estimator, we posit that introducing the

Table 12: Performance comparison on large-scale datasets.

Task	Method	Acc	Bits	Task	Method	Acc	Bits
ogb- arxiv (GCN)	FP32	71.7 ± 0.3	32	(GraphSAGE)	FP32	66.6 ± 1.3	32
	A2Q	71.1 ± 0.3	2.7		MixQ	60.8 ± 2.2	5.0
	+GPF-Plus	70.9 ± 0.3	2.7		+GPF-Plus	61.0 ± 1.6	5.0
	+UniPrompt	71.3 ± 0.4	2.7		+UniPrompt	60.1 ± 1.1	4.9
	+LoRAP	73.6 ± 0.1	2.7		+LoRAP	63.3 ± 2.0	5.0
	MixQ	69.3 ± 0.0	7.1		FP32	33.6 ± 0.4	32
	+GPF-Plus	70.1 ± 0.2	7.1		A2Q	32.7 ± 0.4	2.7
	+UniPrompt	69.4 ± 0.2	7.1		+GPF-Plus	30.4 ± 0.1	2.9
	+LoRAP	71.9 ± 0.1	7.0		+UniPrompt	31.0 ± 0.4	2.9
					+LoRAP	34.2 ± 0.2	2.7

high-precision prompt P facilitates convergence by acting as a continuous relaxation variable. Specifically, the fully differentiable term $P_A P_B^T$ provides a stable gradient pathway that dynamically absorbs high-frequency quantization noise, effectively smoothing the optimization trajectory and guiding the solver away from the poor local minima often inherent to discrete optimization. Empirically, we observe that the loss curves of GPF-LoRAP decrease monotonically without the oscillations typically associated with hyperparameter sensitivity.